Evaluation of Modulation Schemes for Three-Phase to Three-Phase Matrix Converters

Lars Helle, Kim B. Larsen, Allan Holm Jorgensen, Stig Munk-Nielsen, *Member, IEEE*, and Frede Blaabjerg, *Fellow, IEEE*

***Abstract*—This paper presents a method for evaluating different modulation schemes employed with three-phase to three-phase matrix converters. The evaluation method addresses three important modulator characteristics: the output waveform quality, the input waveform quality and the switching losses associated with the modulation schemes. The method is used to evaluate four different modulation strategies, all based on the direct space-vector modulation approach. Further, regarding the switching losses, the paper proposes a new space-vector approach by which the switching losses can be reduced by 15%–35%, depending on the output load angle. This new modulation approach is applicable whenever the output voltage reference is below half the input voltage and the output voltage quality is then superior to that of the conventional space vector modulation scheme. The functionality of the new modulation scheme is validated by both simulations and experimental results and compared to waveforms obtained by using exiting space vector modulation schemes. The output voltage of the proposed scheme turns out to be comparable to the best of the conventional schemes while the input current is more distorted.**

***Index Terms*—Harmonic distortion, matrix converter, pulsewidth modulated (PWM), space-vector modulation, switching losses.**

I. Introduction

In RECENT years, matrix converters for use in induction motor drives have received considerable attention as a competitor to the normally used pulsewidth-modulated voltage-source inverter (PWM-VSI). The matrix converter topology is shown in Fig. 1, where each of the nine switches represents a bidirectional configuration. Compared to the PWM-VSI with diode rectification stage at the input, the matrix converter provides sinusoidal input and output waveforms, bidirectional power flow, controllable input power factor, and a more compact design [1]. On the other hand, the matrix converter can only be linearly modulated to an output voltage equal to 0.866 times the input voltage [2]. Further, the filter design issues are complex and a decoupling between input and output distortions is to some extent limited due to the absence of the dc-link capacitor [3]–[5]. Regarding the converter efficiency, [6] and [7] have performed some general considerations, concluding that at low switching frequencies, the VSI are the most efficient, while at higher switching frequencies, the matrix converter becomes superior. A realistic comparison (if at all possible) should however include a number of design considerations, among these a selection of modulation strategy for both converters. Unfortunately, with regard to modulation strategies, the field of VSI modulation seems quite better explored [8] than the corresponding field of matrix converters. Regarding the VSI, different modulators can be applied by which the switching loss is reduced by up to 50% compared to the normally used modulation schemes [9].

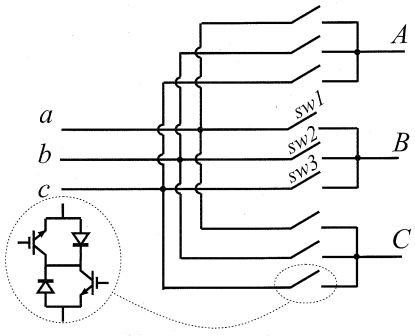

Fig. 1. Matrix converter topology.

Loss reduction in matrix converters has mainly been focused on reducing the number of switchings [10] and on hardware considerations [11]. Moreover, like the performance evaluation of PWM-VSI modulation schemes presented in [8], no similar approach exists for modulation schemes applicable to the matrix converter. The purposes of this paper are as follows:

1) presentation of a new loss reduced space vector modulation approach that is applicable whenever the output voltage reference is below half the input voltage [12];
2) presentation of a performance evaluation method for three-phase to three-phase matrix converter modulation schemes, regarding switching losses, input waveform quality and output waveform quality.

First, the paper reviews the space-vector analysis applied to three-phase to three-phase matrix converters. Then, the conventional space-vector modulation theory for matrix converters is reviewed using the direct approach. From the theory of the conventional direct space-vector modulation, the new switching loss reduced space-vector approach is derived. Some important aspects regarding the switching sequence and the placement of the zero vectors are also discussed for both the conventional scheme and the new reduced switching loss space-vector approach. The remaining part of the paper is dedicated to the development of a tool usable for performance analysis of modulation schemes for matrix converters. The performance analysis

Manuscript received April 2, 2003; revised July 17, 2003. Abstract published on the Internet November 26, 2003.

L. Helle, K. B. Larsen, and A. H. Jorgensen are with Vestas Wind Systems A/S, DK-6950 Ringkøbing, Denmark (e-mail: LAH@vestas.dk).

S. Munk-Nielsen and F. Blaabjerg are with the Institute of Energy Technology, Aalborg University, DK-9220 Aalborg East, Denmark.

Digital Object Identifier 10.1109/TIE.2003.821900

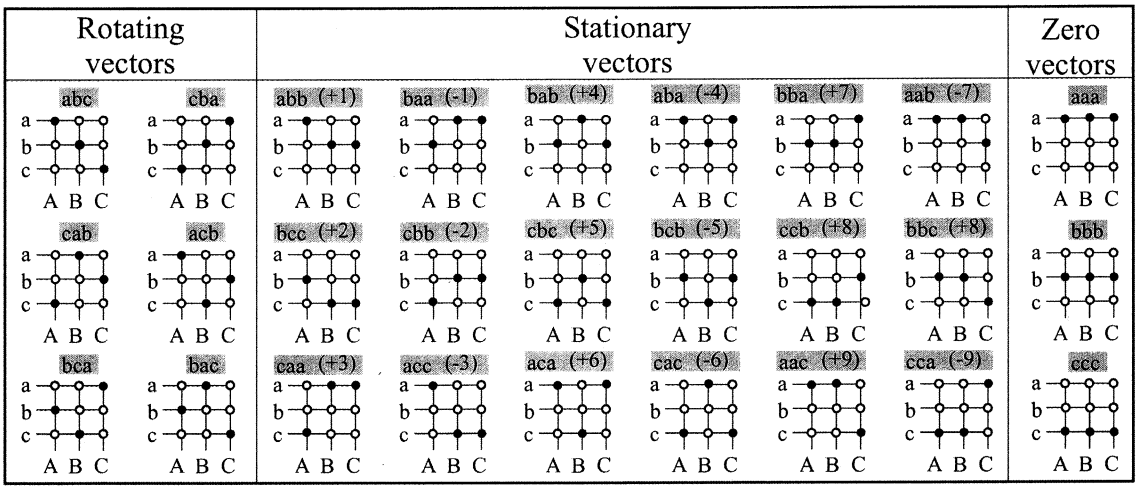

Fig. 2. The 27 allowed switch combinations in a matrix converter.

is divided into three parts concerning the switching losses, the input performance, and the output performance of the different modulation schemes. Finally, in order to show the functionality of the proposed switching loss reduced space vector modulation method and in order to compare the different modulation methods in the time domain, the paper contains simulated and experimental results of different modulation schemes.

II. Vector Analysis of the Switching Combinations

From Fig. 1 it appears that the control of the matrix converter involves 2^9 different switch states. However, since the matrix converter is supplied by voltage sources, the input phases must never be shorted and due to the inductive nature of the load, the output phases must not be left open. Complying with these two basic control rules, only 27 switch combinations are valid. These combinations are shown in Fig. 2. For the space-vector modulation of the matrix converter it is convenient to define the following four space vectors [13]:

$$\underline{V}_{gp} = \frac{2}{3}(v_a + v_b e^{j(2\pi/3)} + v_c e^{j(4\pi/3)}) \quad (1)$$

$$\underline{V}_{rp} = \frac{2}{3}(v_A + v_B e^{j(2\pi/3)} + v_C e^{j(4\pi/3}) \quad (2)$$

$$\underline{I}_{gp} = \frac{2}{3}(i_a + i_b e^{j(2\pi/3)} + i_c e^{j(4\pi/3)}) \quad (3)$$

$$\underline{I}_{rp} = \frac{2}{3}(i_A + i_B e^{j(2\pi/3)} + i_C e^{j(4\pi/3)}) \quad (4)$$

where $\underline{V}_{gp}$ is the space-vector representation for the input phase voltage, $\underline{V}_{rp}$ is the space-vector representation for the output phase voltage, $\underline{I}_{gp}$ is the space-vector representation for the input phase current, and $\underline{I}_{rp}$ is the space-vector representation for the output phase current. Applying (2) on the active switch combinations shown in Fig. 2, it turns out that all these combinations become stationary vectors in the complex space vector plane, but with time varying amplitudes. The output voltage vectors for the active switch combinations are shown in Fig. 3(a). Similarly, by using (3) it appears that the active switch combinations correspond to stationary input current vectors in the complex space vector plane. Due to these properties of the active switch combinations, the well-known space-vector modulation principle can be applied to the matrix converter, although the modulation has to both consider the input current and the output voltage in the same step.

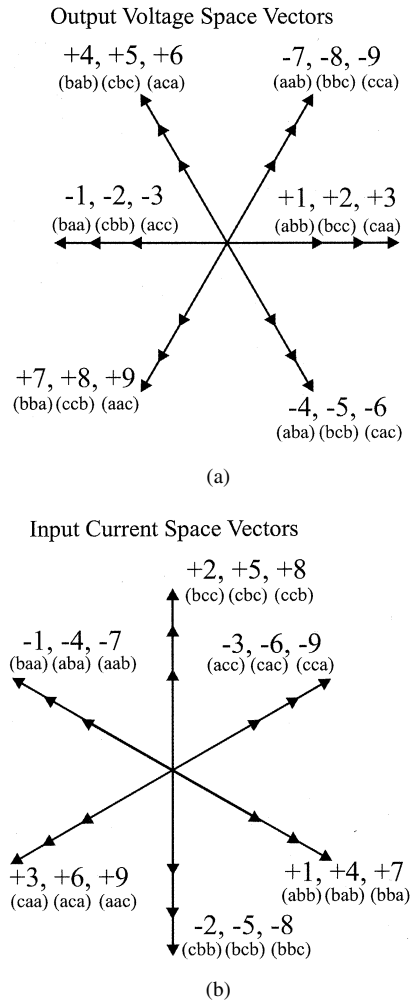

Fig. 3. Space-vector hexagons for the active switch combinations, cf. Fig. 2. (a) Output voltage. (b) Input current.

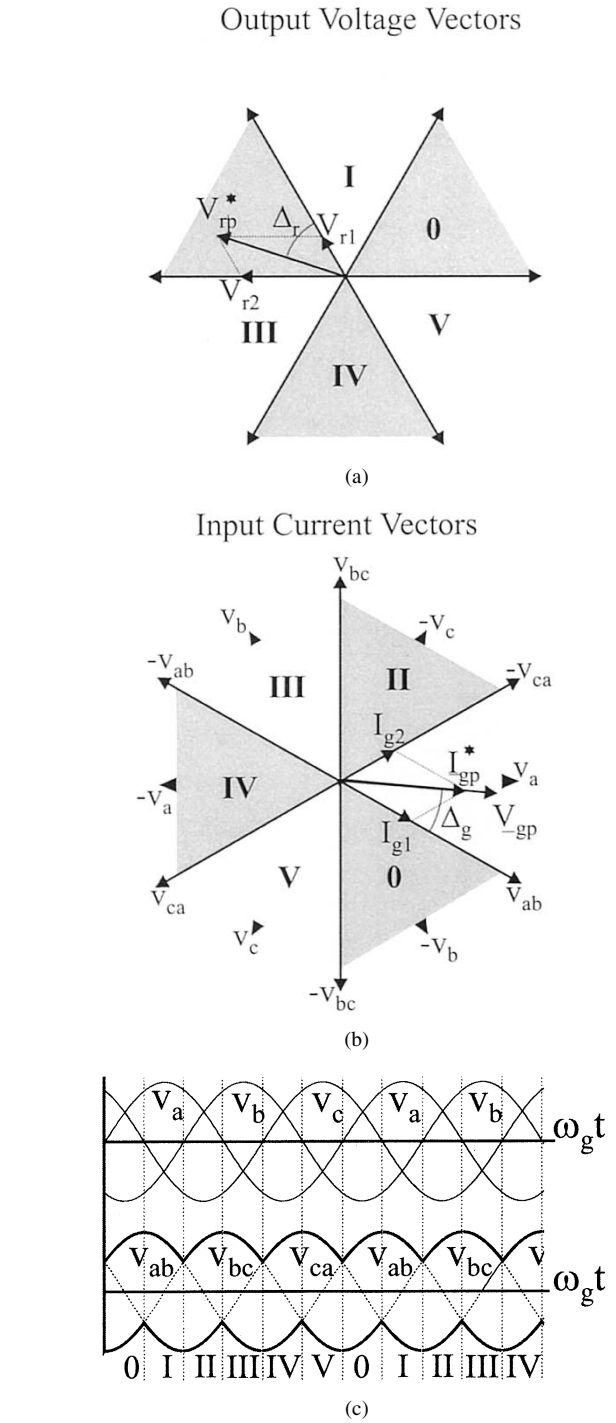

Fig. 4. Angle and sector definitions for the conventional space vector modulation. (a) Output voltage. (b) Input current. (c) Input sector definition in the time domain.

III. Conventional Space-Vector Modulation

A. Vector Time Intervals

In the conventional direct space-vector modulation approach, the sectors are defined as shown in Fig. 4. The input angle Δ_g used in the conventional space-vector modulation is defined as

$$\Delta_g = \mathrm{mod}\left(\omega_g t, \frac{\pi}{3}\right) \tag{5}$$

where $\omega_g t = 0$ is defined as the positive zero crossing of the phase a input voltage ($v_a = \hat{v}_g \cdot \sin(\omega_g t)$). Similarly, the output voltage angle Δ_r is defined as

$$\Delta_r = \mathrm{mod}\left(\omega_r t + \frac{\pi}{6}, \frac{\pi}{3}\right) \tag{6}$$

where ω_r is the angular speed of the output voltage reference vector and $\omega_r t = 0$ is defined as the positive zero crossing of the phase A output voltage ($v_A^\star = \hat{v}_r^\star \cdot \sin(\omega_r t)$).

For an arbitrary sector location of the output voltage reference $\underline{V}_{rp}^\star$ and the input voltage vector $\underline{V}_{gp}$, the following equations can be derived using that $\underline{V}_{rp}^\star = \underline{V}_{r1} + \underline{V}_{r2}$:

$$\begin{aligned}
\underline{V}_{r1} &= |\underline{V}_{rp}^\star| \cdot \sin\left(\frac{\pi}{3} - \Delta_r\right) \cdot \frac{2}{\sqrt{3}} \\
&= \delta_1 \cdot \cos\left(\Delta_g - \frac{\pi}{3}\right) |\underline{V}_{gp}| \cdot \frac{2}{\sqrt{3}} \\
&\quad - \delta_2 \cdot \cos\left(\Delta_g - \pi\right) |\underline{V}_{gp}| \cdot \frac{2}{\sqrt{3}} \\
\underline{V}_{r2} &= |\underline{V}_{rp}^\star| \cdot \sin\left(\Delta_r\right) \cdot \frac{2}{\sqrt{3}} \\
&= \delta_3 \cdot \cos\left(\Delta_g - \frac{\pi}{3}\right) \cdot |\underline{V}_{gp}| \cdot \frac{2}{\sqrt{3}} \\
&\quad - \delta_4 \cdot \cos\left(\Delta_g - \pi\right) \cdot |\underline{V}_{gp}| \cdot \frac{2}{\sqrt{3}}
\end{aligned} \tag{7}$$

where $\delta_{1..4}$ are the on-time durations for the four applied vectors. In each input sector, only the two line–line voltages with the highest amplitudes are used. This is illustrated in the lower part of Fig. 4. By similar considerations the input current vectors are calculated, using that ($\underline{I}_{gp}^\star = \underline{I}_{g1} + \underline{I}_{g2}$)

$$\begin{aligned}
\underline{I}_{g1} &= |\underline{I}_{gp}^\star| \cdot \sin\left(\frac{\pi}{3} - \Delta_g\right) \cdot \frac{2}{\sqrt{3}} \\
&= \delta_2 \cdot i_x \cdot \frac{2}{\sqrt{3}} - \delta_4 \cdot i_y \cdot \frac{2}{\sqrt{3}} \\
\underline{I}_{g2} &= |\underline{I}_{gp}^\star| \cdot \sin\left(\Delta_g\right) \cdot \frac{2}{\sqrt{3}} \\
&= \delta_1 \cdot i_x \cdot \frac{2}{\sqrt{3}} - \delta_3 \cdot i_y \cdot \frac{2}{\sqrt{3}}
\end{aligned} \tag{8}$$

where i_x and i_y are the instantaneous values of two output phase currents. Assuming that the output currents are sinusoidal and symmetrically distributed, the relation between i_x and i_y are

$$\begin{cases} i_x &= \hat{i}_{rp} \cdot \sin(\omega_r t) \\ i_y &= \hat{i}_{rp} \cdot \sin\left(\omega_r t \pm \frac{2\pi}{3}\right) \end{cases}$$
$$\Downarrow$$
$$i_y = i_x \cdot \frac{\sin\left(\omega_r t \pm \frac{2\pi}{3}\right)}{\sin(\omega_r t)}. \tag{9}$$

Combining (8) and (9) and rearranging, the following output-current-dependent expression is obtained:

$$\begin{aligned}
0 = &-\frac{\delta_1}{\sin(\Delta_g)} - \frac{\delta_4 \cdot \sin\left(\omega_r t \pm \frac{2\pi}{3}\right)}{\sin\left(\frac{\pi}{3} - \Delta_g\right) \cdot \sin(\omega_r t)} \\
&+ \frac{\delta_2}{\sin\left(\frac{\pi}{3} - \Delta_g\right)} + \frac{\delta_3 \cdot \sin\left(\omega_r t \pm \frac{2\pi}{3}\right)}{\sin(\omega_r t) \cdot \sin(\Delta_g)}.
\end{aligned} \tag{10}$$

TABLE I
SWITCHING THE CONVENTIONAL SPACE-VECTOR MODULATION

→Rec	Sector 0				Sector I				Sector II				Sector III				Sector IV				Sector V			
↓Inv	δ_1	δ_2	δ_3	δ_4	δ_1	δ_2	δ_3	δ_4	δ_1	δ_2	δ_3	δ_4	δ_1	δ_2	δ_3	δ_4	δ_1	δ_2	δ_3	δ_4	δ_1	δ_2	δ_3	δ_4
0	abb	cbb	aab	ccb	acc	abb	aac	aab	bcc	acc	bbc	aac	baa	bcc	bba	bbc	caa	baa	cca	bba	cbb	caa	ccb	cca
I	aab	ccb	bab	bcb	aac	aab	cac	bab	bbc	aac	cbc	cac	bba	bbc	aba	cbc	cca	bba	aca	aba	ccb	cca	bcb	aca
II	bab	bcb	baa	bcc	cac	bab	caa	baa	cbc	cac	cbb	caa	aba	cbc	abb	cbb	aca	aba	acc	abb	bcb	aca	bcc	acc
III	baa	bcc	bba	bbc	caa	baa	cca	bba	cbb	caa	ccb	cca	abb	cbb	aab	ccb	acc	abb	aac	aab	bcc	acc	bbc	aac
IV	bba	bbc	aba	cbc	cca	bba	aca	aba	ccb	cca	bcb	aca	aab	ccb	bab	bcb	aac	aab	cac	bab	bbc	aac	cbc	cac
V	aba	cbc	abb	cbb	aca	aba	acc	abb	bcb	aca	bcc	acc	bab	bcb	baa	bcc	cac	bab	caa	baa	cbc	cac	cbb	caa

In order to achieve solutions for the modulation functions $\delta_{1..4}$ which are independent of the output current position, (10) can be separated into the following two equations:

$$\begin{aligned} 0 &= \delta_2 \cdot \sin(\Delta_g) - \delta_1 \cdot \sin\left(\frac{\pi}{3} - \Delta_g\right) \\ 0 &= \delta_3 \cdot \sin\left(\frac{\pi}{3} - \Delta_g\right) - \delta_4 \cdot \sin(\Delta_g). \end{aligned} \tag{11}$$

Solving (7) and (11) for the modulation functions $\delta_{0..4}$ gives

$$\begin{aligned} \delta_1 &= \frac{2 \cdot |\underline{V}^{\star}_{rp}|}{\sqrt{3} \cdot |\underline{V}_{gp}|} \cdot \sin(\Delta_g) \cdot \sin\left(\frac{\pi}{3} - \Delta_r\right) \\ \delta_2 &= \frac{2 \cdot |\underline{V}^{\star}_{rp}|}{\sqrt{3} \cdot |\underline{V}_{gp}|} \cdot \sin\left(\frac{\pi}{3} - \Delta_g\right) \cdot \sin\left(\frac{\pi}{3} - \Delta_r\right) \\ \delta_3 &= \frac{2 \cdot |\underline{V}^{\star}_{rp}|}{\sqrt{3} \cdot |\underline{V}_{gp}|} \cdot \sin(\Delta_g) \cdot \sin(\Delta_r) \\ \delta_4 &= \frac{2 \cdot |\underline{V}^{\star}_{rp}|}{\sqrt{3} \cdot |\underline{V}_{gp}|} \cdot \sin\left(\frac{\pi}{3} - \Delta_g\right) \cdot \sin(\Delta_r) \\ \delta_0 &= 1 - (\delta_1 + \delta_2 + \delta_3 + \delta_4). \end{aligned} \tag{12}$$

It should, however, be noted that the modulation functions at any time instant are limited by the following constraint:

$$\delta_{0..4} >= 0. \tag{13}$$

Using only the two line–line voltages with maximum amplitudes, the sector-dependent switch combinations for each duty-cycle function $\delta_{1..4}$ are summarized in Table I. The sector notation in Table I refers to the sector location in Fig. 4.

B. Modulation Index

When comparing different modulation strategies for one type of converter, it is often convenient to normalize the output voltage to some reference voltage. This normalized voltage quantity is termed the modulation index M. The choice of reference voltage can be arbitrary and in the literature different choices exist which lead to some confusion. In this context, the choice of reference voltage is chosen in such a way that the modulation index becomes unity at the boundary between the linear modulation range and over modulation for the conventional modulation method. Hence, from (12) and (13) the modulation index becomes

$$M = \frac{2 \cdot |\underline{V}^{\star}_{rp}|}{\sqrt{3} \cdot |\underline{V}_{gp}|}. \tag{14}$$

Equation (14) shows that the maximum output reference voltage $|\widehat{V}^{\star}_{rp}|$ is limited to $\sqrt{3}/2$ of the input phase voltage.

IV. MODIFIED SPACE-VECTOR MODULATION

The main idea of the modified space-vector modulation [12] is to make use of the minimum line–line voltage (contrary to the conventional space vector modulation which utilizes the two maximum line–line voltages) whenever the output voltage reference is less than half of the input voltage. The advantages of this new modulation strategy are that the harmonic content of the output voltages are reduced and, additionally, the switching losses are decreased. A disadvantage of the proposed modulation strategy is that the harmonic current spectrum on the input side of the converter is changed.

A. Vector Time Intervals

Fig. 5 shows the output hexagons and the input hexagons for the modified space vector modulation approach. The line–line voltages used within each of the sectors are indicated by the increased line width in the lower part of Fig. 5. The procedure for deriving the duty-cycle functions for the modified space vector modulation approach is almost similar to the procedure in the conventional space vector modulation. However, for completion of the modulation description, the derivation of the modified duty-cycle function is given below.

The input angle Δ_g used in the modified space vector modulation is defined as, cf. Fig. 5,

$$\Delta_g = \mathrm{mod}\left(\left(\omega_g t + \frac{\pi}{6}\right), \frac{\pi}{3}\right) \tag{15}$$

where $\omega_g t = 0$ is defined as the positive zero crossing of the phase a input voltage ($v_a = \hat{v}_g \cdot \sin(\omega_g t)$). The output voltage angle Δ_r is defined as

$$\Delta_r = \mathrm{mod}\left(\left(\omega_r t + \frac{\pi}{6}\right), \frac{\pi}{3}\right). \tag{16}$$

For an arbitrary sector location of the output voltage reference and the input voltage, the following equations can be derived:

$$\begin{aligned} V_{r1} &= |\underline{V}^{\star}_{rp}| \cdot \sin\left(\frac{\pi}{3} - \Delta_r\right) \cdot \frac{2}{\sqrt{3}} \\ &= -\delta_1 \cdot \cos\left(\Delta_g + \frac{\pi}{2}\right) |\underline{V}_{gp}| \cdot \frac{2}{\sqrt{3}} \\ &\quad - \delta_2 \cdot \cos\left(\frac{5\pi}{6} - \Delta_g\right) |\underline{V}_{gp}| \cdot \frac{2}{\sqrt{3}} \\ V_{r2} &= |\underline{V}^{\star}_{rp}| \cdot \sin(\Delta_r) \cdot \frac{2}{\sqrt{3}} \\ &= -\delta_3 \cdot \cos\left(\Delta_g + \frac{\pi}{2}\right) |\underline{V}_{gp}| \cdot \frac{2}{\sqrt{3}} \\ &\quad - \delta_4 \cdot \cos\left(\frac{5\pi}{6} - \Delta_g\right) |\underline{V}_{gp}| \cdot \frac{2}{\sqrt{3}}. \end{aligned} \tag{17}$$

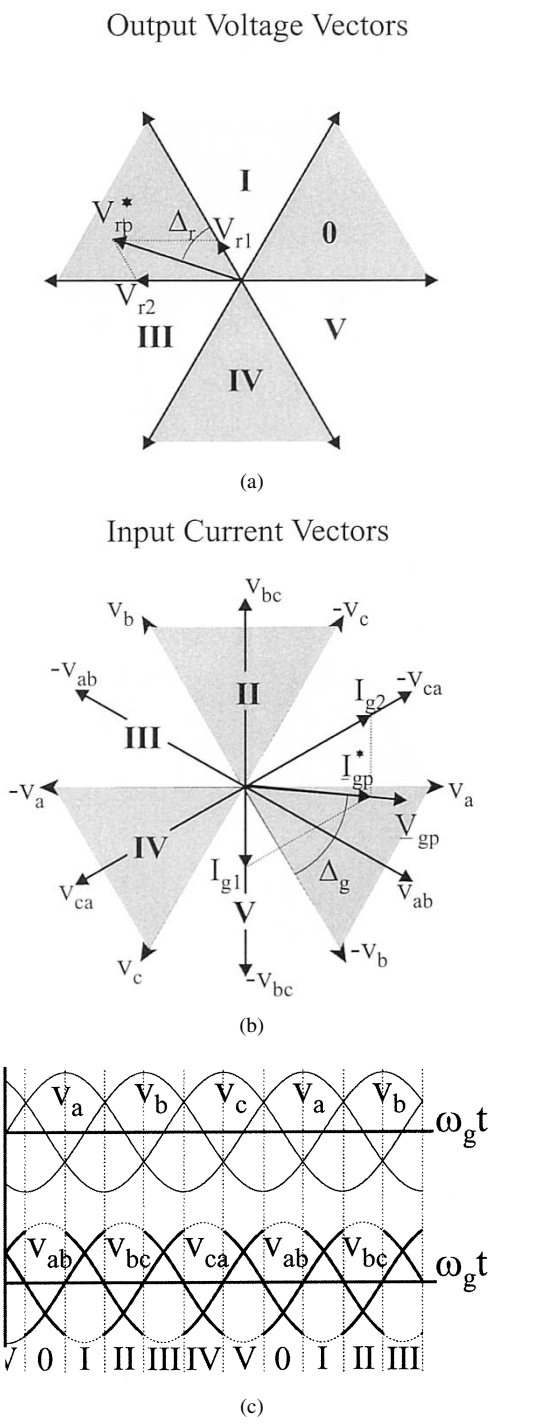

Fig. 5. Angle and sector definitions for the modified space-vector modulation. (a) Output voltage. (b) Input current. (c) Input sector definition in the time domain.

Similarly, the current reference $|\underline{I}^{\star}_{gp}|$ can be obtained by

$$\begin{aligned} I_{g1} &= |\underline{I}^{\star}_{gp}| \cdot \cos(\Delta_g) \cdot \frac{2}{\sqrt{3}} \\ &= \delta_2 \cdot i_x \cdot \frac{2}{\sqrt{3}} - \delta_4 \cdot i_y \cdot \frac{2}{\sqrt{3}} \\ I_{g2} &= |\underline{I}^{\star}_{gp}| \cdot \cos\left(\frac{\pi}{3} - \Delta_g\right) \cdot \frac{2}{\sqrt{3}} \\ &= \delta_1 \cdot i_x \cdot \frac{2}{\sqrt{3}} - \delta_3 \cdot i_y \cdot \frac{2}{\sqrt{3}}. \end{aligned} \tag{18}$$

Using the relation in (9), the modulation functions $\delta_{0..4}$ for the modified modulation approach can be derived as

$$\begin{aligned} \delta_1 &= \frac{2 \cdot |\underline{V}^{\star}_{rp}|}{\sqrt{3} \cdot |\underline{V}_{gp}|} \cos\left(\frac{\pi}{3} - \Delta_g\right) \cdot \sin\left(\frac{\pi}{3} - \Delta_r\right) \\ \delta_2 &= \frac{2 \cdot |\underline{V}^{\star}_{rp}|}{\sqrt{3} \cdot |\underline{V}_{gp}|} \cos(\Delta_g) \cdot \sin\left(\frac{\pi}{3} - \Delta_r\right) \\ \delta_3 &= \frac{2 \cdot |\underline{V}^{\star}_{rp}|}{\sqrt{3} \cdot |\underline{V}_{gp}|} \cos\left(\frac{\pi}{3} - \Delta_g\right) \cdot \sin(\Delta_r) \\ \delta_4 &= \frac{2 \cdot |\underline{V}^{\star}_{rp}|}{\sqrt{3} \cdot |\underline{V}_{gp}|} \cos(\Delta_g) \cdot \sin(\Delta_r) \\ \delta_0 &= 1 - (\delta_1 + \delta_2 + \delta_3 + \delta_4). \end{aligned} \tag{19}$$

It should be noted that the modulation functions at any time instant are limited by the constraint in (13). Table II shows the sector-dependent switch combinations for the modified modulation approach. The sector notation in Table II refers to the sector location in Fig. 5.

B. Modulation Index

For comparison, it is convenient to retain the modulation index expression defined in (14). Taking the constraint in (13) into account, it is found that the boundary between linear modulation and over modulation occurs at a modulation index of 0.577. Hence, the maximum output reference voltage $|V^{\star}_{rp}|$ for the modified space-vector approach is limited to half of the input voltage.

V. Double-Sided Vector Sequences

Like the modulation of the VSI, the vector sequences and the placement of the zero vectors have a high influence on the performance and the efficiency of the matrix converter. In the first papers concerning space-vector modulation, single-sided modulation was used [14], but at the expense of only a slight increase in the number of branch switch overs (BSOs) per switching period, double-sided modulation has become the preferred method. In double-sided modulation, the switching period is divided into two equal periods and in both these periods the four selected active vectors are applied. In the last of the two periods, the sequence order is reversed. The zero vectors can be applied anywhere in the switching sequence. Due to the better harmonic performance at the input side and at the output side, only double-sided modulation is considered in this paper. Specifically, the following four double-sided modulation strategies will be treated:

- conventional double-sided modulation (8 BSOs) [15];
- double-sided modulation for the modified space-vector algorithm (8 BSOs) [12];
- conventional double-sided modulation with distributed zero vectors (10 BSOs) [16];
- double-sided modulation with distributed zero vectors for the modified space-vector algorithm (10 BSOs).

A. Conventional Modulation (8 BSOs)

In the conventional modulation presented in [15] the switching sequence for the conventional modulation was

TABLE II
SWITCHING THE MODIFIED SPACE-VECTOR MODULATION

→Rec	Sector 0				Sector I				Sector II				Sector III				Sector IV				Sector V			
↓Inv	δ_1	δ_2	δ_3	δ_4	δ_1	δ_2	δ_3	δ_4	δ_1	δ_2	δ_3	δ_4	δ_1	δ_2	δ_3	δ_4	δ_1	δ_2	δ_3	δ_4	δ_1	δ_2	δ_3	δ_4
0	acc	cbb	aac	ccb	bcc	abb	bbc	aab	baa	acc	bba	aac	caa	bcc	cca	bbc	cbb	baa	ccb	bba	abb	caa	aab	cca
I	aac	ccb	cac	bcb	bbc	aab	cbc	bab	bba	aac	aba	cac	cca	bbc	aca	cbc	ccb	bba	bcb	aba	aab	cca	bab	aca
II	cac	bcb	caa	bcc	cbc	bab	cbb	baa	aba	cac	abb	caa	aca	cbc	acc	cbb	bcb	aba	bcc	abb	bab	aca	baa	acc
III	caa	bcc	cca	bbc	cbb	baa	ccb	bba	abb	caa	aab	cca	acc	cbb	aac	ccb	bcc	abb	bbc	aab	baa	acc	bba	aac
IV	cca	bbc	aca	cbc	ccb	bba	bcb	aba	aab	cca	bab	aca	aac	ccb	cac	bcb	bbc	aab	cbc	bab	bba	aac	aba	cac
V	aca	cbc	acc	cbb	bcb	aba	bcc	abb	bab	aca	baa	acc	cac	bcb	caa	bcc	cbc	bab	cbb	baa	aba	cac	abb	caa

optimized with regards to the BSOs per switching fundamental, giving a minimum number of 8 BSOs. Following this switching procedure, there is still one degree of freedom left and that is the position of the zero-vector within the switching sequence. The zero vector could either be applied in the beginning of the sequence or in the center of the sequence. Regarding the converter efficiency (and the emission of common-mode voltage [17]), the amplitude of the switched voltage, when changing to/from the zero-vector state can be used to determine the zero-vector placement, cf. the lower part of Fig. 4. Hence, for even sector sums, the half of the switching sequence is

$$\delta_0 \xrightarrow[v_{ab}]{i_C} \delta_3 \xrightarrow[v_{ab}]{i_B} \delta_1 \xrightarrow[v_{ca}]{i_A} \delta_2 \xrightarrow[v_{bc}]{i_B} \delta_4 \ldots, \qquad \text{if} \quad \Delta_g < \frac{\pi}{6} \tag{20}$$

$$\delta_3 \xrightarrow[v_{ab}]{i_B} \delta_1 \xrightarrow[v_{ca}]{i_A} \delta_2 \xrightarrow[v_{bc}]{i_B} \delta_4 \xrightarrow[v_{bc}]{i_C} \delta_0 \ldots, \qquad \text{if} \quad \Delta_g > \frac{\pi}{6} \tag{21}$$

and for odd sector sums, half of the switching sequence is

$$\delta_0 \xrightarrow[v_{ca}]{i_A} \delta_1 \xrightarrow[v_{ca}]{i_B} \delta_3 \xrightarrow[v_{bc}]{i_C} \delta_4 \xrightarrow[v_{ab}]{i_B} \delta_2 \ldots, \qquad \text{if} \quad \Delta_g < \frac{\pi}{6} \tag{22}$$

$$\delta_1 \xrightarrow[v_{ca}]{i_B} \delta_3 \xrightarrow[v_{bc}]{i_C} \delta_4 \xrightarrow[v_{ab}]{i_B} \delta_2 \xrightarrow[v_{ab}]{i_A} \delta_0 \ldots, \qquad \text{if} \quad \Delta_g > \frac{\pi}{6}. \tag{23}$$

For each BSO in (20)–(23) the switched currents and line–line voltages are shown. The shown currents and voltages are valid for sector 0_{rec}–0_{inv} and I_{rec}–0_{inv}, respectively. By use of Table I, the switched voltages and switched currents for an arbitrary sector location can be determined. This will be used when evaluating the switching losses of the conventional double-sided modulation method.

B. Modified Space-Vector Modulation (8 BSOs)

By inspection of Table II it appears that the switching sequences of the modified modulation strategy are to be changed in order to obtain the minimum of 8 BSOs per switching fundamental. Hence, for even sector sums, half of the switching sequence should be

$$\delta_3 \xrightarrow[v_{ca}]{i_B} \delta_1 \xrightarrow[v_{ca}]{i_A} \delta_0 \xrightarrow[v_{bc}]{i_C} \delta_4 \xrightarrow[v_{bc}]{i_B} \delta_2 \ldots \tag{24}$$

which assures 8 BSOs per switching fundamental. For odd sector sums, half of the switching sequence should be

$$\delta_1 \xrightarrow[v_{bc}]{i_B} \delta_3 \xrightarrow[v_{ab}]{i_C} \delta_0 \xrightarrow[v_{bc}]{i_A} \delta_2 \xrightarrow[v_{ab}]{i_B} \delta_4 \ldots. \tag{25}$$

Compared to the conventional method it appears that only the two minimum line–line voltages are switched, which presumably decreases the switching losses. The switched currents and voltages listed in (24) and (25) are valid for sector 0_{rec}–0_{inv} and I_{rec}–0_{inv} respectively. By the use of Table II the switched voltages and currents can be determined for an arbitrary sector location of the output reference vector and the input current vector.

C. Conventional Modulation With Distributed Zero Vectors (10 BSOs)

The third method takes advantage of that the switching sequence order can be used to increase the switching frequency seen from the input side by distributing the zero vectors throughout the switching period. This is especially advantageous when considering the input filter design. However, this is achieved at the expense of a higher number of BSOs per switching fundamental. In [16], different distributions of the zero vector are discussed and it is concluded that the most significant improvements are obtained by distributing the zero vector at the beginning and in the center of the switching sequence. This doubles the dominant switching frequency seen from the input side at the expense of only two additional switchings per switching fundamental. With the constraint of only one BSO per switch-state shift, there is no degree of freedom left in the order of the switching sequence. According to [16], half of the switching sequence for even sector sums is

$$\delta_0 \xrightarrow[v_{ab}]{i_C} \delta_3 \xrightarrow[v_{ab}]{i_B} \delta_1 \xrightarrow[v_{ca}]{i_A} \delta_2 \xrightarrow[v_{bc}]{i_B} \delta_4 \xrightarrow[v_{bc}]{i_C} \delta_0 \ldots \tag{26}$$

and for odd sector sums

$$\delta_0 \xrightarrow[v_{ca}]{i_A} \delta_1 \xrightarrow[v_{ca}]{i_B} \delta_3 \xrightarrow[v_{bc}]{i_C} \delta_4 \xrightarrow[v_{ab}]{i_B} \delta_2 \xrightarrow[v_{ab}]{i_A} \delta_0 \ldots. \tag{27}$$

The switched currents and voltages listed in (26) and (27) are valid for sector 0_{rec}–0_{inv} and I_{rec}–0_{inv}, respectively.

D. Modified Space-Vector Modulation With Distributed Zero Vectors (10 BSOs)

Adopting the method from [16] for use in the modified modulation approach is not as simple as for the conventional modulation due to a higher degree of freedom when ordering the switching sequence. According to the sequences in (24) and (25) the additional zero vector could be applied in either the beginning of the sequence or in the center of the sequence. In order to explain the differences in the zero-vector placement, half of the switching sequence for sector 0_{rec}–0_{inv} is listed in (28) where the optional zero-vector placement is marked with the δ_0' and δ_0'', respectively,

$$\delta_0' \xrightarrow[v_{ca}]{i_C} \delta_3 \xrightarrow[v_{ca}]{i_B} \delta_1 \xrightarrow[v_{ca}]{i_A} \delta_0 \xrightarrow[v_{bc}]{i_C} \delta_4 \xrightarrow[v_{bc}]{i_B} \delta_2 \xrightarrow[v_{bc}]{i_A} \delta_0'' \ldots. \tag{28}$$

From (28) it appears that the positioning of the zero vector can be done either with regard to the switched current or with regard to the switched voltage.

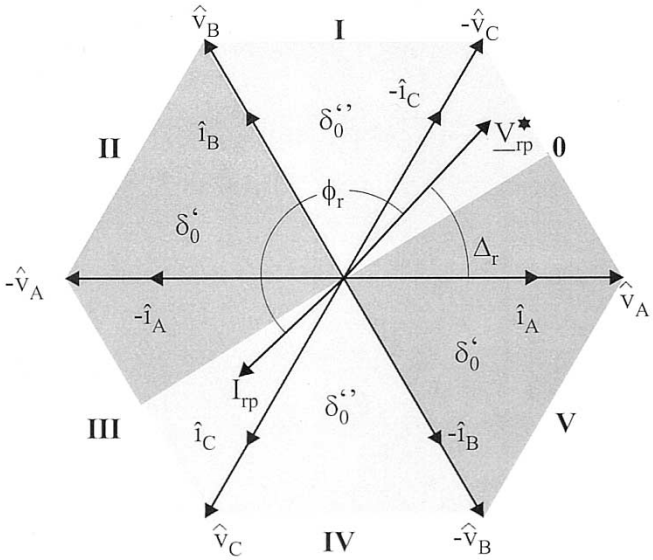

Fig. 6. Output current and output voltage space-vector diagram.

1) Switched Voltage: Regarding the switched voltage, it appears from the lower part of Fig. 5 that half of the switching sequence for even sectors should be

$$\delta_0 \xrightarrow[v_{ca}]{i_C} \delta_3 \xrightarrow[v_{ca}]{i_B} \delta_1 \xrightarrow[v_{ca}]{i_A} \delta_0 \xrightarrow[v_{bc}]{i_C} \delta_4 \xrightarrow[v_{bc}]{i_B} \delta_2 \ldots, \qquad \text{if } \Delta_g < \frac{\pi}{6} \quad (29)$$

$$\delta_3 \xrightarrow[v_{ca}]{i_B} \delta_1 \xrightarrow[v_{ca}]{i_A} \delta_0 \xrightarrow[v_{bc}]{i_C} \delta_4 \xrightarrow[v_{bc}]{i_B} \delta_2 \xrightarrow[v_{bc}]{i_A} \delta_0 \ldots, \qquad \text{if } \Delta_g > \frac{\pi}{6} \quad (30)$$

in order to assure that the lowest voltage is switched when applying the zero vector. For odd sectors, the sequence should be

$$\delta_0 \xrightarrow[v_{bc}]{i_A} \delta_1 \xrightarrow[v_{bc}]{i_B} \delta_3 \xrightarrow[v_{ab}]{i_C} \delta_0 \xrightarrow[v_{bc}]{i_A} \delta_2 \xrightarrow[v_{ab}]{i_B} \delta_4 \ldots, \qquad \text{if } \Delta_g < \frac{\pi}{6} \quad (31)$$

$$\delta_1 \xrightarrow[v_{bc}]{i_B} \delta_3 \xrightarrow[v_{ab}]{i_C} \delta_0 \xrightarrow[v_{bc}]{i_A} \delta_2 \xrightarrow[v_{ab}]{i_B} \delta_4 \xrightarrow[v_{ab}]{i_C} \delta_0 \ldots, \qquad \text{if } \Delta_g > \frac{\pi}{6}. \quad (32)$$

The modulation method described by the sequences in (29)–(32) is in the further denoted *modified modulation (10 BSOs) with distributed zero vectors (SV)*, where the abbreviation *SV* indicates that the modulation regards the switched voltage.

2) Switched Current: Regarding the switched current, the modified modulation with distributed zero vectors can adopt some of the features from the discontinuous modulation strategies of the VSI. In other words, the placement of the zero vector can be determined such that the minimum current is switched. By this, the optional placement of the zero vector becomes dependent of the angle ϕ_r between output current and output voltage. This is illustrated in Fig. 6, where the output current and output phase voltage space-vector diagram is shown. For illustration purposes, the output voltage reference vector $\underline{V}^{\star}_{rp}$ is located in sector 0 and the angle between the output voltage reference and the output current is ϕ_r. In order to assure that the minimum output current is switched when switching to/from the zero-vector state, the switching sequence in (28) should be altered between the δ_0' and the δ_0'' sequence in accordance with the output current position in Fig. 6.

Generalizing to an arbitrary sector location of the output current vector half of the vector sequence for even sector sums becomes

$$\delta_0 \xrightarrow[v_{ca}]{i_C} \delta_3 \xrightarrow[v_{ca}]{i_B} \delta_1 \xrightarrow[v_{ca}]{i_A} \delta_0 \xrightarrow[v_{bc}]{i_C} \delta_4 \xrightarrow[v_{bc}]{i_B} \delta_2, \text{ if } \begin{cases} -\frac{\pi}{3} < (\Delta_r + \phi_r) < \frac{\pi}{6} \\ \frac{2\pi}{3} < (\Delta_r + \phi_r) < \frac{7\pi}{6} \end{cases} \quad (33)$$

$$\delta_3 \xrightarrow[v_{ca}]{i_B} \delta_1 \xrightarrow[v_{ca}]{i_A} \delta_0 \xrightarrow[v_{bc}]{i_C} \delta_4 \xrightarrow[v_{bc}]{i_B} \delta_2 \xrightarrow[v_{bc}]{i_A} \delta_0, \text{ if } \begin{cases} \frac{\pi}{6} < (\Delta_r + \phi_r) < \frac{2\pi}{3} \\ \frac{7\pi}{6} < (\Delta_r + \phi_r) < \frac{5\pi}{3} \end{cases} \quad (34)$$

and for odd sector sums the switching sequence becomes

$$\delta_1 \xrightarrow[v_{bc}]{i_B} \delta_3 \xrightarrow[v_{ab}]{i_C} \delta_0 \xrightarrow[v_{bc}]{i_A} \delta_2 \xrightarrow[v_{ab}]{i_B} \delta_4 \xrightarrow[v_{ab}]{i_C} \delta_0, \text{ if } \begin{cases} -\frac{\pi}{3} < (\Delta_r + \phi_r) < \frac{\pi}{6} \\ \frac{2\pi}{3} < (\Delta_r + \phi_r) < \frac{7\pi}{6} \end{cases} \quad (35)$$

$$\delta_0 \xrightarrow[v_{bc}]{i_A} \delta_1 \xrightarrow[v_{bc}]{i_B} \delta_3 \xrightarrow[v_{ab}]{i_C} \delta_0 \xrightarrow[v_{bc}]{i_A} \delta_2 \xrightarrow[v_{ab}]{i_B} \delta_4, \text{ if } \begin{cases} \frac{\pi}{6} < (\Delta_r + \phi_r) < \frac{2\pi}{3} \\ \frac{7\pi}{6} < (\Delta_r + \phi_r) < \frac{5\pi}{3} \end{cases}. \quad (36)$$

Following the switching sequences in (33)–(36), the modulator needs information about the instantaneous angle between output voltage and output current. However, it is easily realized, that the angle ϕ_r can be preset to a fixed value representing the steady-state nominal value of the load angle.

The modulation method described by the sequences in (33)–(36) is in the further denoted *modified modulation (10 BSOs) with distributed zero vectors (SC)*, where the abbreviation *SC* indicates that the modulation regards the switched current.

VI. Switching Losses

Assuming that the switching devices of the matrix converter have a linear current and voltage turn-on and turn-off characteristic with respect to time and counting only for the fundamental component of the output current, the switching losses p_{sw} of the matrix converter can be analytically modeled as [18]

$$p_{\mathrm{sw}} \propto v_{\mathrm{sw}} \cdot i_{\mathrm{sw}} \cdot (T_{\mathrm{on}} + T_{\mathrm{off}}) \cdot f_{\mathrm{sw}} \quad (37)$$

where v_{sw} is the switched voltage, i_{sw} is the switched current, f_{sw} is the switching frequency and T_{on} and T_{off} is the turn-on and turn-off times for the switching devices. For further simplification, (37) is normalized to the product of the peak output current $\hat{i}_r$, the peak value of the switched voltage v_{gL} (which is the peak line–line voltage at the supply grid), the switching frequency, and the device characteristics. The normalized switching loss function $p_{\mathrm{sw},n}$ yields

$$p_{\mathrm{sw},n} \propto \frac{p_{\mathrm{sw}}}{\hat{v}_{gL} \cdot \hat{i}_r \cdot (T_{\mathrm{on}} + T_{\mathrm{off}}) \cdot f_{\mathrm{sw}}}. \quad (38)$$

Using the different switching sequences, the normalized per-carrier switching losses may be calculated for arbitrary sector locations of the output voltage reference vector, the input current reference vector, and the output current vector (it is provided that the input current vector and the input voltage vector are synchronized, i.e., the input current is in phase with the input voltage). Fig. 7 shows the normalized switching losses for the conventional modulation method, cf. (20)–(23), when the output current and output voltage are in phase.

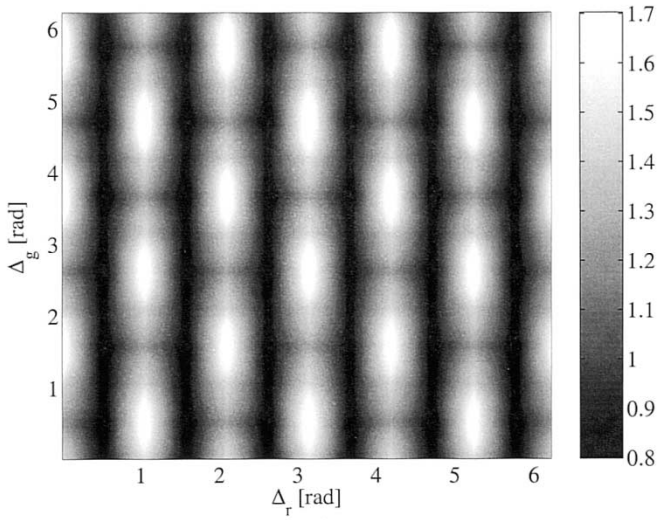

Fig. 7. Contour plot of the per-carrier switching losses of the conventional modulation method for $\phi_r = 0$. The losses are plotted against the angles Δ_g and Δ_r.

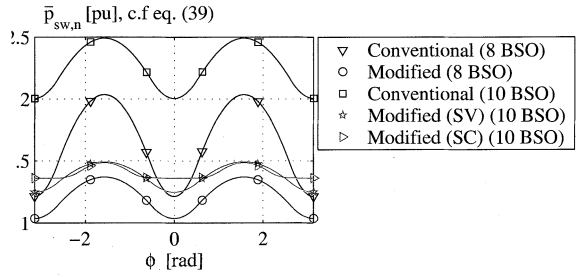

Fig. 8. Switching losses of the four different modulation functions for the matrix converter.

From Fig. 7 it appears that the switching losses averaged over a common time period for the input frequency and the output frequency depends on the actual course over the surface. However, considering a general case, where the input frequency and the output frequency have no common time period, the average switching losses are calculated by integrating over the entire surface. Hence, to evaluate the different modulation methods with regards to the switching losses the following normalized switching loss function is defined:

$$\bar{p}_{\mathrm{sw},n} \propto \frac{1}{4\pi^2}\int_0^{2\pi}\int_0^{2\pi}(p_{\mathrm{sw},n})d\Delta_g d\Delta_r. \tag{39}$$

By the use of (39) the switching loss functions of the different modulators can be calculated for different load cases, i.e., different angle ϕ_r between output voltage and output current. Fig. 8 shows the normalized switching loss functions for the different modulators as a function of the angle ϕ_r.

VII. Harmonic Performance

When modulating the matrix converter in order to synthesize a desired output voltage and input current, harmonics are introduced at integer multiples of the switching frequency and at the side bands of all these frequencies. The harmonic content depends on the chosen modulation scheme and since this undesired frequency content causes torque ripple and additional copper losses in e.g., a motor load and increases the demands to the input filter, it is convenient to have a method to compare the harmonic behavior of different modulation schemes.

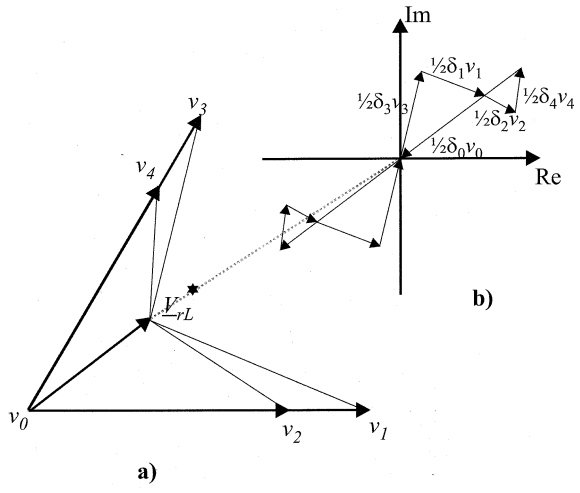

Fig. 9. Illustration of the per-carrier harmonic flux trajectory. (a) Output voltage hexagon (first segment). (b) Resulting harmonic flux trajectory (conventional 8-BSO modulation scheme.

A. Output Voltage

To evaluate the output voltage quality, the harmonic flux is considered [8]. In the Nth carrier cycle the harmonic flux $\tilde{\psi}$ is calculated by

$$\tilde{\psi} = \int_{NT_{\mathrm{sw}}}^{(N+1)T_{\mathrm{sw}}} (\underline{V}_{rp} - \underline{V}^{\star}_{rp})dt \tag{40}$$

where $\underline{V}_{rp}$ is a stationary output voltage vector and T_{sw} is the carrier period. To generalize the performance characterization, the per-carrier harmonic flux error $\tilde{\psi}$ in (40), is normalized to the product of the nominal output voltage amplitude $|\hat{\underline{V}}_{rp}|$ and half the carrier period. That is,

$$\tilde{\psi}_n = \frac{2}{T_{\mathrm{sw}}|\hat{\underline{V}}_{rp}|}\cdot\tilde{\psi}. \tag{41}$$

The normalized per-carrier cycle rms value of the harmonic flux $\tilde{\psi}_{\mathrm{RMS},n}$ can now be calculated by

$$\langle\tilde{\psi}_{\mathrm{RMS},n}\rangle_{T_{\mathrm{sw}}} = \sqrt{\int_0^1 \left(\tilde{\psi}_n\cdot\tilde{\psi}_n^*\right)dt} \tag{42}$$

where $\tilde{\psi}_n^*$ is the complex conjugate of $\tilde{\psi}_n$. Fig. 9 illustrates the harmonic flux trajectory for the conventional (8 BSOs) modulation. Fig. 10 shows the per-carrier cycle rms value of the harmonic flux as a function of the input angle Δ_g and the output angle Δ_r. The harmonic flux is plotted for a modulation index of 1. Evaluating for a general case, where the input frequency

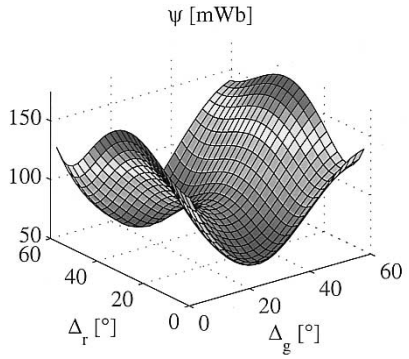

Fig. 10. Per-carrier cycle rms value of the harmonic flux as a function of the input and output angle for the conventional 8-BSO modulation strategy.

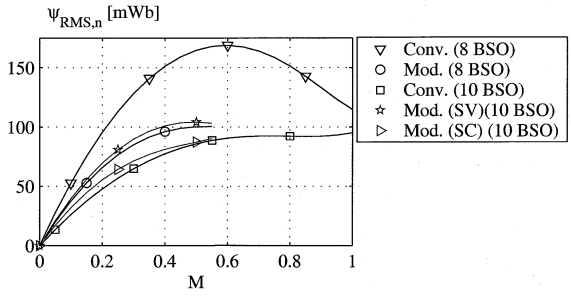

Fig. 11. Harmonic flux as a function of the modulation index, cf. (14).

and the output frequency have no common time period, the rms value of the harmonic flux is obtained by integrating over the entire surface. The rms value of the harmonic flux is calculated by

$$\tilde{\psi}_{\mathrm{RMS},n} = \sqrt{\frac{1}{4\pi^2}\int_0^{2\pi}\int_0^{2\pi}\left(\langle\tilde{\psi}_{\mathrm{RMS},n}\rangle_{T_{\mathrm{sw}}}\right)^2 d\Delta_g\, d\Delta_r}. \quad (43)$$

Fig. 11 shows the rms value of the harmonic flux as a function of the modulation index.

It should be noted that for $\cos(\phi_g) \neq 1$ at the input, all curves in Fig. 11 would be changed.

B. Input Current

When the input current to the matrix converter is modulated, the instantaneous error between the input current reference vector $\underline{I}^{\star}_{gp}$ and the chosen stationary input current vector $\underline{I}_{gp}$, results in a high-frequency harmonic current. This harmonic current generates high stress on the input filter capacitors and has to be considered when designing the input filter for the matrix converter. Like for the voltage quality, the harmonic current content depends on the modulation method and hence an evaluation method is needed in order to compare the input waveform quality of the different modulation schemes.

In principle, the evaluation of the input current follows the same procedure as for the output voltage, however the evaluation parameter is changed from harmonic flux to harmonic charge $\tilde{Q}$. Further, the evaluation of the input current becomes

TABLE III
SIMULATION CONDITIONS (MATRIX CONVERTER)

Switching frequency	f_{sw}	3550	[Hz]
Power factor	$\cos(\phi_g)$	1	
Input inductance	L_f	300	[μH]
Input capacitor	C_f	61.0	[μF]
Input voltage (l-l)	V_g	400	[V]
Modulation index	M	0.58	
Input frequency	f_g	50	[Hz]
Output frequency	f_r	25	[Hz]

TABLE IV
SIMULATION CONDITIONS (INDUCTION MOTOR)

Nominal power	P_{im}	15	[kW]
Power factor	$\cos(\phi_r)$	0.84	
Pole pair	N	2	
Stator resistance	R_s	0.36	[Ω]
Rotor resistance	R_r	0.26	[Ω]
Leakage inductance	L_s	2.2	[mH]
Leakage inductance	L_r	2.2	[mH]
Mag. inductance	L_m	46.6	[mH]

a little more complex than the evaluation of the output voltage due to the fact that the amplitudes of the stationary input current vectors are affected by the output load angle ϕ_r. In the N^{th} carrier cycle the harmonic charge $\tilde{Q}$ is calculated by

$$\tilde{Q} = \int_{NT_{\mathrm{sw}}}^{(N+1)T_{\mathrm{sw}}} (\underline{I}_{gp} - \underline{I}^{\star}_{gp})dt \quad (44)$$

where $\underline{I}_{gp}$ is a stationary input current vector. The amplitude of the per-carrier harmonic charge is a function of the input current angle, the output voltage angle, the modulation depth, and the output load angle ϕ_r. To obtain a comparison, independent of the switching frequency and power level, the harmonic charge in (44) is normalized by

$$\tilde{Q}_n = \frac{4\tilde{Q}}{\sqrt{3}\cdot T_{\mathrm{sw}}\cdot \hat{i}_{rp}} \quad (45)$$

where $\hat{i}_{rp}$ is the amplitude of the output current. The normalized per-carrier cycle rms value of the harmonic charge $\tilde{Q}_{\mathrm{RMS},n}$ can be calculated by

$$\langle\tilde{Q}_{\mathrm{RMS},n}\rangle_{T_{\mathrm{sw}}} = \sqrt{\int_0^1 \left(\tilde{Q}_n \cdot \tilde{Q}_n^*\right) dt} \quad (46)$$

where $\tilde{Q}_n^*$ is the complex conjugate of $\tilde{Q}_n$. Evaluating for a general case, where the input frequency and the output frequency has no common time period, the rms value of the harmonic charge is obtained by integrating over the entire surface. The rms value of the harmonic charge is calculated by

$$\tilde{Q}_{RMS,n} = \sqrt{\frac{1}{4\pi^2}\int_0^{2\pi}\int_0^{2\pi}\left(\langle\tilde{Q}_{RMS,n}\rangle_{T_{\mathrm{sw}}}\right)^2 d\Delta_g\, d\Delta_r}. \quad (47)$$

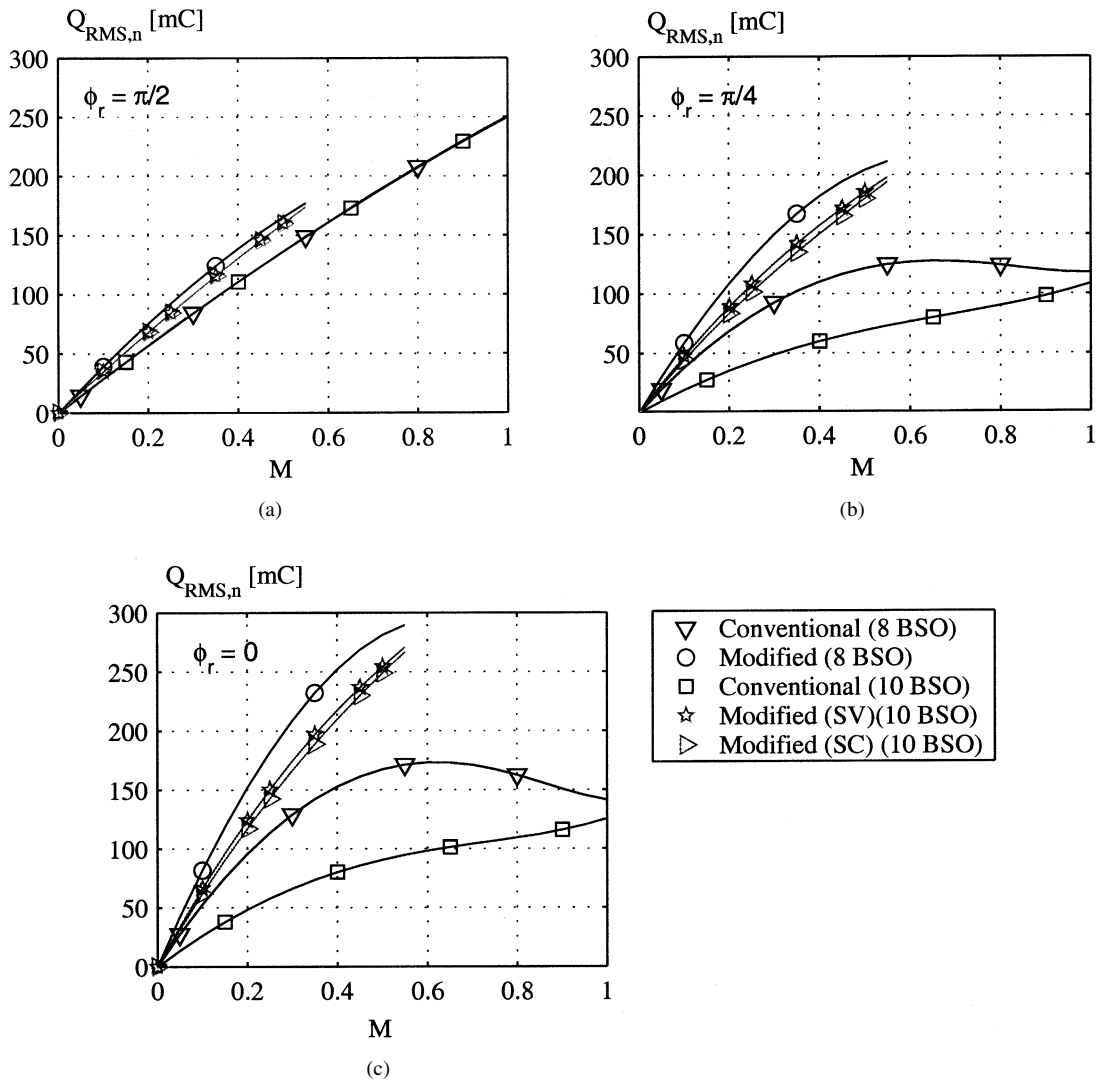

Fig. 12. Normalized harmonic charge distortion as a function of the modulation index, cf. (14) for different load angles. (a) load angle equals $\pi/2$. (b) Load angle equals $\pi/4$. (c) Load angle equals 0.

TABLE V
TOTAL HARMONIC CURRENT DISTORTION (THD$_i$) (%)

f_r	M	Conv. (8 BSO)		Mod. (8 BSO)		Conv. (10 BSO)		Mod. (SV)(10 BSO)	
		Input	Output	Input	Output	Input	Output	Input	Output
15.0	0.35	7.30	5.57	13.01	3.69	2.86	2.87	12.20	3.85
20.0	0.46	8.87	5.87	15.84	3.72	3.42	3.11	14.33	3.87
25.0	0.58	9.14	5.57	16.68	3.43	4.03	3.07	15.93	3.49
30.0	0.69	8.30	5.10	-	-	4.37	2.99	-	-
35.0	0.81	7.15	3.95	-	-	4.66	2.60	-	-
40.0	0.92	6.10	3.06	-	-	4.89	2.39	-	-
42.5	0.98	5.87	2.73	-	-	5.00	2.34	-	-

Fig. 12 shows the normalized harmonic charge $\tilde{Q}_{RMS}$ versus the modulation index for different load angles.

VIII. SIMULATION AND TEST RESULTS

A. Test Setup

To validate the functionality of the proposed modified space vector approach and to compare the different modulation schemes in the time domain, a flexible laboratory test setup was built. Tables III and IV show the characteristics of the test and simulation setup and specifies the conditions used.

B. Simulated Results

Fig. 13 shows the simulated waveforms of the conventional (8 BSOs) modulation scheme and the modified (8 BSOs) modulation scheme. Fig. 14 shows the simulated waveforms for the

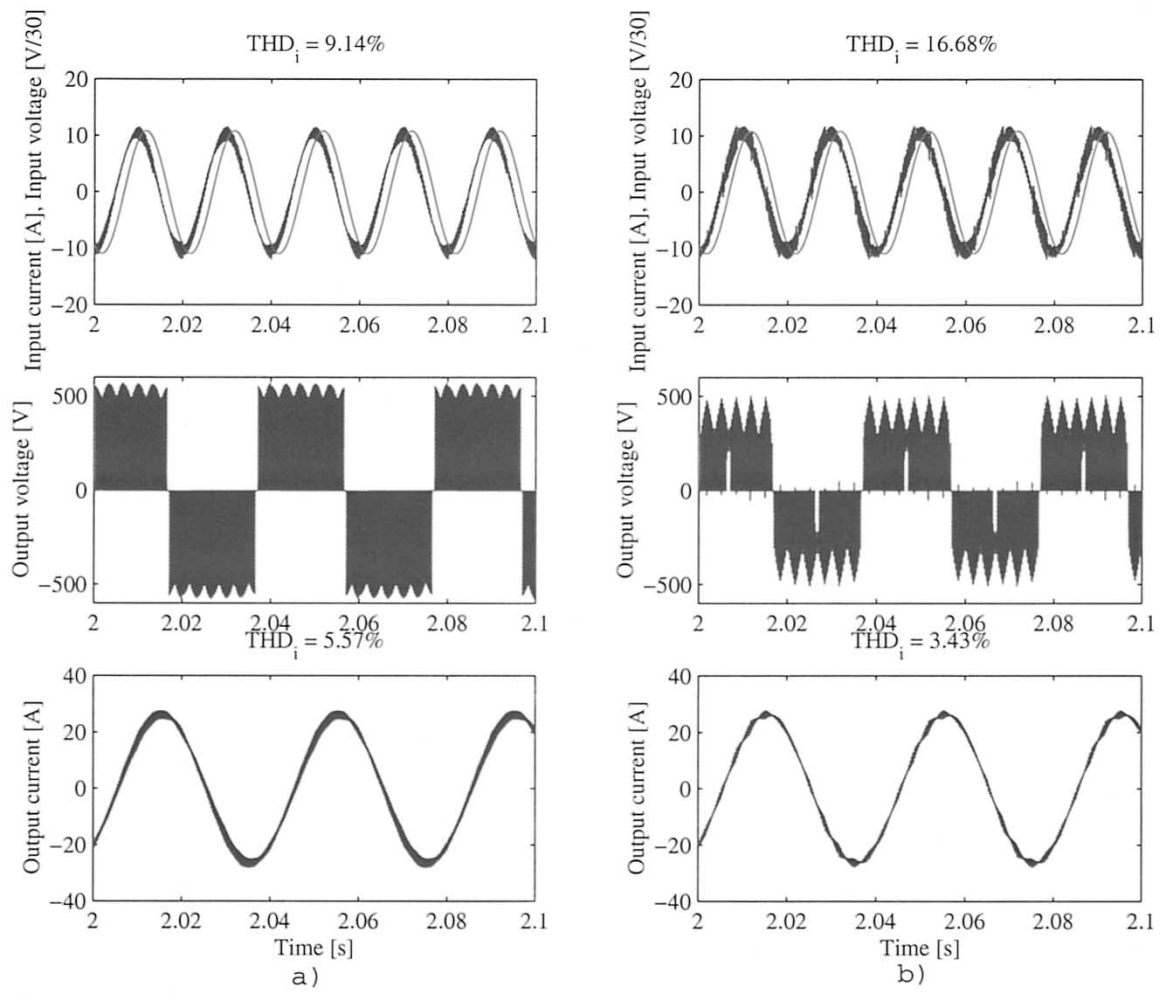

Fig. 13. Simulation results. (a) Conventional modulation method (8 BSOs). (b) Modified modulation method (8 BSOs). The upper curves show the input currents and the input voltage, the curves in the middle show the output voltages (line–line) and the lower plots show the output currents. Simulation conditions are given in Tables III and IV.

conventional (10 BSO) modulation scheme and the modified (10 BSOs) modulation scheme (SV). For each of the simulated currents, the corresponding total harmonic current distortion (THD$_i$) is calculated (upper right corner of the trace). Besides the conditions simulated in Figs. 13 and 14, Table V shows the total harmonic current distortion in the entire speed range. From the results in Figs. 13, 14, and Table V, it appears that both with regards to the output voltage quality and the input current quality, the conventional (10 BSOs) modulation scheme shows the best results. Regarding the 8-BSO modulation schemes, the proposed solution shows better output performance than the conventional method while regarding the input performance the conventional scheme is superior.

C. Experimental Results

Figs. 15–17 show the experimentally obtained waveforms. Fig. 15 shows the measured waveforms for the conventional 8-BSO modulation scheme, Fig. 16 shows it for the conventional 10-BSO scheme, and Fig. 17 represents the modified 8-BSO scheme.

IX. Conclusion

This paper has presented a new loss reduced modulation scheme for three-phase to three-phase matrix converters. The new modulation scheme is applicable whenever the output voltage reference is below half the input voltage. The proposed scheme reduces the switching losses by 15%-35% dependent on the load angle at the output of the converter. To evaluate the proposed modulation method and matrix converter modulation schemes in general, an evaluation method is proposed, regarding the three crucial modulation properties: the switching losses, the output voltage quality, and the input current quality. Four different modulation schemes are evaluated. To demonstrate the functionality of the loss reduced modulation method and to some extent validate the proposed evaluation method, a matrix converter motor drive was simulated, using the four considered modulation schemes. It turned out (both from the analytical method and from the simulations) that regarding the input and output waveform quality, the conventional (10 BSOs) modulation strategy was superior while regarding the switching losses, the new modified (8 BSOs) modulation was the most efficient. Finally, the functionality of some of the discussed

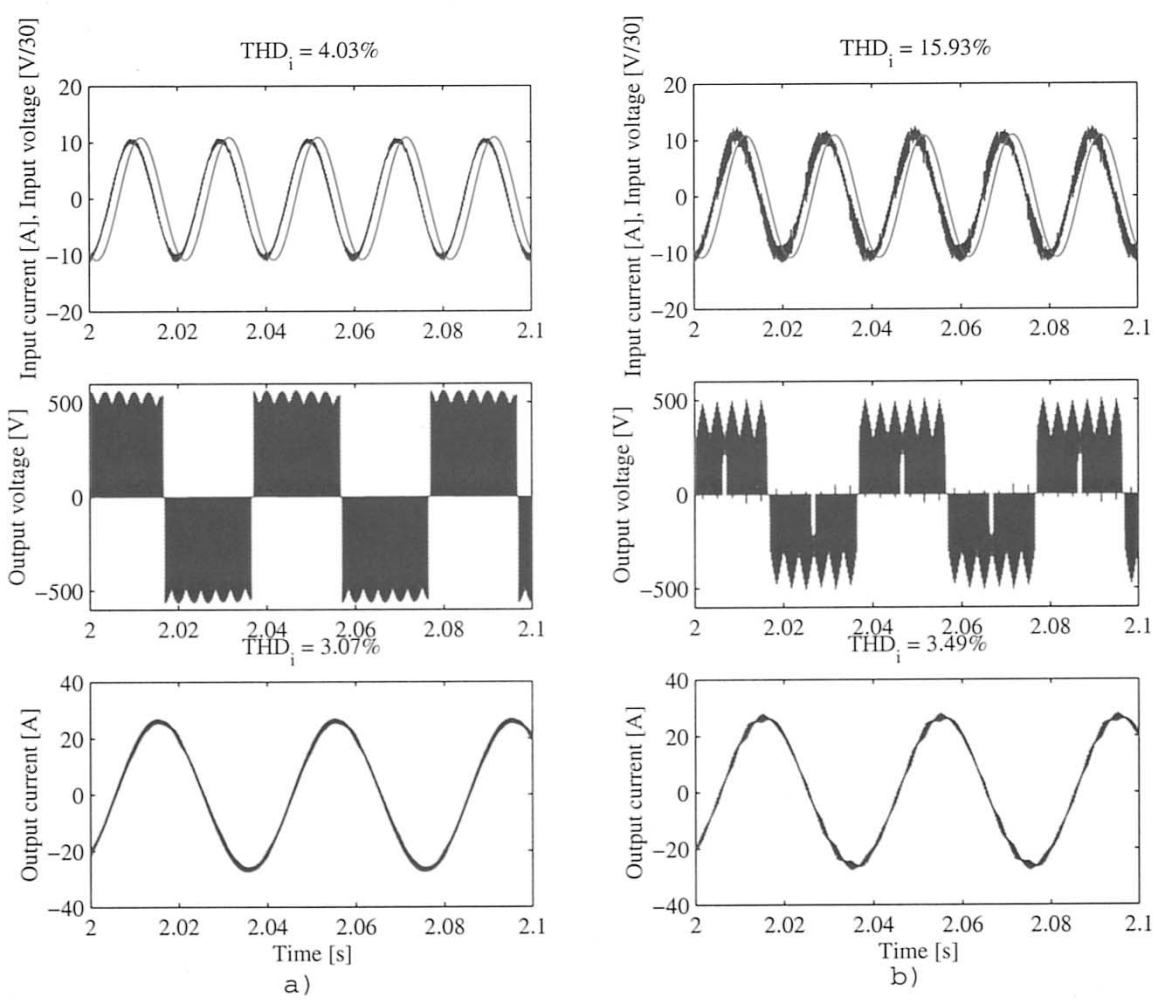

Fig. 14. Simulation results. (a) Conventional modulation method (10 BSOs). (b) Modified modulation method (10-BSO SV). The upper curves show the input currents and the input voltage, the curves in the middle show the output voltages (line–line) and the lower plots show the output currents. Simulation conditions are given in Tables III and IV.

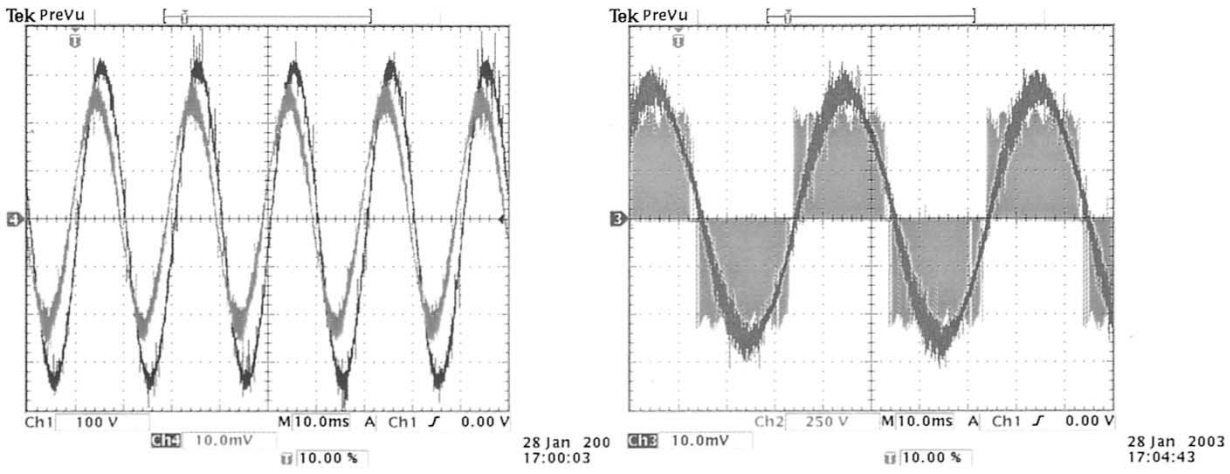

(a) (b)

Fig. 15. Measured waveforms for the conventional 8-BSO scheme. (a) Input current (5 A/10 mV) and input voltage. (b) Output current and output voltage (10 A/10 mV).

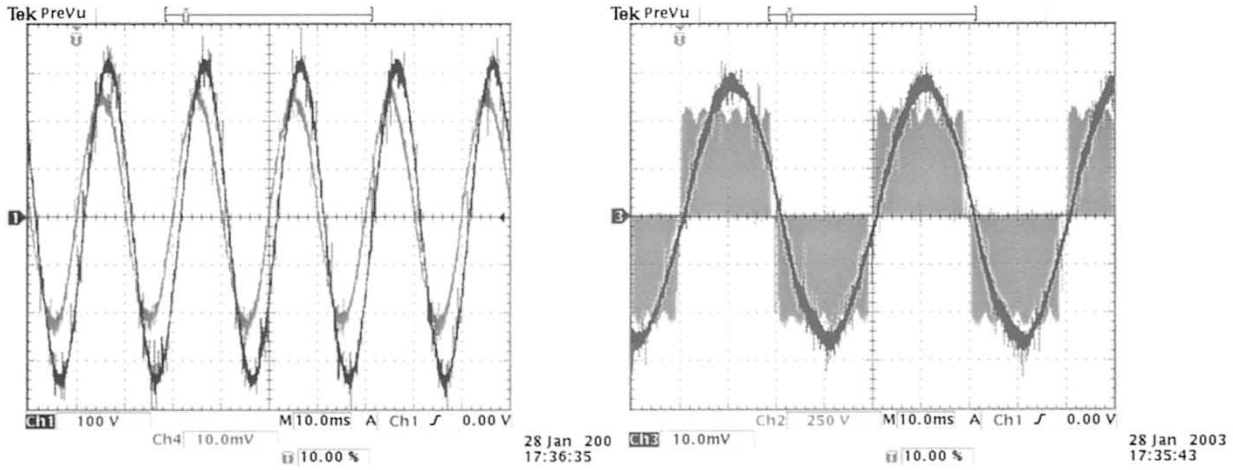

(a) (b)

Fig. 16. Measured waveforms for the conventional 10-BSO scheme. (a) Input current (5 A/10 mV) and input voltage. (b) Output current and output voltage (10 A/10 mV).

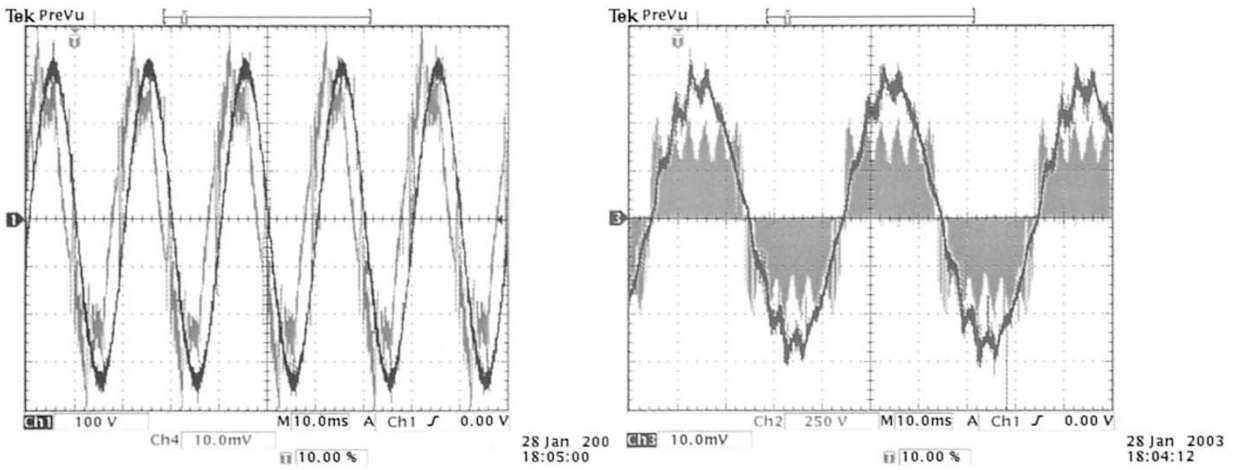

(a) (b)

Fig. 17. Measured waveforms for the modified 8-BSO scheme. (a) Input current and input voltage (5 A/10 mV). (b) Output current and output voltage (10 A/10 mV).

modulation schemes were demonstrated by experimental results.

REFERENCES

[1] D. Casadei, G. Serra, and A. Tani, "Reduction of the input current harmonic content in matrix converters under input/output unbalance," *IEEE Trans. Ind. Electron.*, vol. 45, pp. 401–411, June 1998.

[2] A. Alesina and M. G. B. Venturini, "Analysis and design of optimum-amplitude nine-switch direct AC-AC converters," *IEEE Trans. Power Electron.*, vol. 4, pp. 101–112, Jan. 1989.

[3] P. Nielsen, D. Casadei, G. Serra, and A. Tani, "Evaluation of the input current quality by three different modulation strategies for SVM controlled matrix converters with input voltage unbalance," in *Proc. PEDES'96*, vol. 2, 1996, pp. 794–800.

[4] B. Ooi and M. Kazerani, "Elimination of the waveform distortions in the voltage-source-converter type matrix converter," in *Conf. Rec. IEEE-IAS Annu. Meeting*, vol. 3, 1995, pp. 2500–2504.

[5] D. Casadei, G. Serra, and A. Tani, "Reduction of the input current harmonic content in matrix converter under input/output unbalance," in *Proc. IECON'95*, vol. 1, 1995, pp. 457–462.

[6] P. Nielsen, "The matrix converter for an induction motor drive," Ph.D. dissertation, Inst. Energy Technol., Aalborg Univ., Aalborg East, Denmark, 1996.

[7] P. W. Wheeler and D. A. Grant, "A low loss matrix converter for AC variable-speed drives," in *Proc. EPE Conf.*, vol. 5, 1993, pp. 27–32.

[8] A. M. Hava, R. J. Kerkman, and T. A. Lipo, "Simple analytical and graphical methods for carrier-based PWM-VSI drives," *IEEE Trans. Power Electron.*, vol. 14, pp. 49–61, Jan. 1999.

[9] ——, "A high performance generalized discontinuous PWM algorithm," in *Proc. PEC'97*, vol. 2, 1997, pp. 886–894.

[10] P. Nielsen, F. Blaabjerg, and J. K. Pedersen, "Space vector modulated matrix converter with minimized number of switchingsand a feedforward compensation of input voltage unbalance," in *Proc. PEDES'96*, vol. 2, 1996, pp. 833–839.

[11] C. Pan, T. Chen, and J. Shieh, "A zero switching loss matrix converter," *Proc. IEEE PESC'93*, pp. 545–550, 1993.

[12] L. Helle and S. Munk-Nielsen, "A new loss reduced modulation strategy for matrix converters," in *Proc. IEEE PESC*, vol. 2, 2001, pp. 1102–1107.

[13] L. Huber and D. Borojević, "Space vector modulated three-phase to three-phase matrix converter with input power factor correction," *IEEE Trans. Ind. Applicat.*, vol. 31, pp. 1234–1246, Nov./Dec. 1995.

[14] D. Casadei, G. Grandi, G. Serra, and A. Tani, "Space vector control of a matrix converter with unity input power factor and sinusoidal input/output waveforms," in *Proc. EPE Conf.*, vol. 7, 1993, pp. 170–175.

[15] P. Nielsen, F. Blaabjerg, and J. K. Pedersen, "New protection issues of a matrix converter – Design considerations for adjustable speed drives," *IEEE Trans. Ind. Applicat.*, vol. 35, pp. 1150–1161, Sept./Oct. 1999.

[16] C. Klumpner, I. Boldea, F. Blaabjerg, and P. Nielsen, "A new modulator for matrix converters allowing for the reduction of input current ripple," in *Proc. OPTIM Conf.*, vol. 2, 2000, pp. 487–492.

[17] H. J. Cha and P. Enjeti, "An approach to reduce common mode voltage in matrix converter," in *Conf. Rec. IEEE-IAS Annu. Meeting*, vol. 1, 2002, pp. 432–437.

[18] O. Al-Naseem, R. W. Ericson, and P. Carlin, "Prediction of switching loss variation by averaged switch modeling," in *Proc. IEEE APEC*, vol. 1, 2000, pp. 242–248.

Lars Helle was born in Odense, Denmark, in 1972. He received the M.Sc.EE and Ph.D. degrees from the Institute of Energy Technology, Aalborg University, Aalborg East, Denmark, in 1998 and 2002, respectively.

During the Ph.D program, he contributed to the technical report "Conceptual Survey of Generators and Power Electronics for Wind Turbines" from the Research Center Risoe and to the book *Control in Power Electronics* (New York, Academic, 2002), edited by M.P. Kazmierkowski, R. Krishnan, F. Blaabjerg. He is currently with the Danish wind turbine manufacturer Vestas Wind Systems A/S, Ringkøbing, Denmark, where he is working with new energy conversion concepts. His research areas include power converters, modulation techniques, and electrical machines.

Kim B. Larsen was born in Randers, Denmark, in 1976. He received the M.Sc.EE degree from the Institute of Energy Technology, Aalborg University, Aalborg East, Denmark, in 2001.

From 2001 to 2002, he was a Research Assistant at the Institute of Energy Technology, Aalborg University. Since January 2002, he has been with Vestas Wind Systems A/S, Ringkøbing, Denmark, where he is currently working with the design and control of drive trains in wind turbines. His main research areas are control methods and different topologies and modulation strategies for power converters.

Allan Holm Jorgensen was born in Spentrup, Denmark. He received the M.Sc.EE degree from the Institute of Energy Technology, Aalborg University, Aalborg East, Denmark, in 2001.

From 2001 to 2002, he was a Research Assistant at the Institute of Energy Technology, Aalborg University, working with converter topologies and converter control. He is currently with Vestas Wind Systems A/S, Ringkøbing, Denmark, working with design and control of converters in wind turbines. His main research areas are power semiconductors, different converter topologies, and modulation strategies for power converters.

Stig Munk-Nielsen (S'92–M'97) was born in 1965. He received the M.Sc.EE and Ph.D. degrees from the Institute of Energy Technology, Aalborg University, Aalborg East, Denmark, in 1991 and 1997, respectively.

Since January 1999, he has been an Associate Professor at Aalborg University. His main research areas are resonant inverters, power converter topologies, modulation techniques, control of electrical machines, simulation of power electronic systems, and characterization of new power semiconductor devices.

Frede Blaabjerg (S'86-M'88–SM'97–F'02) was born in Erslev, Denmark, in 1963. He received the M.Sc. E.E. from Aalborg University, Aalborg East, Denmark in 1987, and the Ph.D. degree from the Institute of Energy Technology, Aalborg University, in 1995.

He was with ABB-Scandia, Randers, from 1987 to 1988. In 1992, he became an Assistant Professor at Aalborg University, where, in 1996, he became an Associate Professor and, in 1998, he became a Full Professor of Power Electronics and Drives. In 2000, he was a Visiting Professor at the University of Padova, Italy, as well a part-time Programme Research Leader at the Research Center Risoe, working on wind turbines. In 2002, he was a Visiting Professor at Curtin University of Technology, Perth, Australia. His research areas are power electronics, static power converters, ac drives, switched reluctance drives, modeling, characterization of power semiconductor devices and simulation, wind turbines, and green power inverters. He is engaged in more than ten research projects with industry, including the Danfoss Professor Programme in Power Electronics and Drives. He is the author or coauthor of more than 300 publications in his research fields, including the book *Control in Power Electronics* (New York: Academic, 2002). He has served as a member of the Danish Technical Research Council since 1997 and, in 2001, he became Chairman. He is Chairman of the Danish Small Satellite programme and the Center Contract Committee which support collaboration between universities and industry.

Dr. Blaabjerg is a member of the European Power Electronics and Drives Association and the Industrial Drives, Industrial Power Converter, and Power Electronics Devices and Components Committees of the IEEE Industry Applications Society. He is also an Associate Editor of the IEEE TRANSACTIONS ON INDUSTRY APPLICATIONS, IEEE TRANSACTIONS ON POWER ELECTRONICS, *Journal of Power Electronics*, and the Danish journal *Elteknik*. He became a Member of the Danish Academy of Technical Science in 2001. He has served as a Member of the Danish Technical Research Council since 1997 and, in 2001, he became Chairman. He is Chairman of the Danish Small Satellite Programme and the Center Contract Committee which support collaboration between universities and industry. He became a Member of the Danish Academy of Technical Science in 2001. In 2002, he became a Member of the Board of the Danish Research Councils. He received the 1995 Angelos Award for his contribution in modulation technique and control of electric drives, and an Annual Teacher Prize from Aalborg University, also in 1995. In 1998, he received the Outstanding Young Power Electronics Engineer Award from the IEEE Power Electronics Society. He has received four IEEE Prize paper awards during the last five years. He received the C.Y. O'Connor Fellowship from Perth, Australia, in 2002 and the Statoil Prize in 2003 for his contributions to power electronics.